

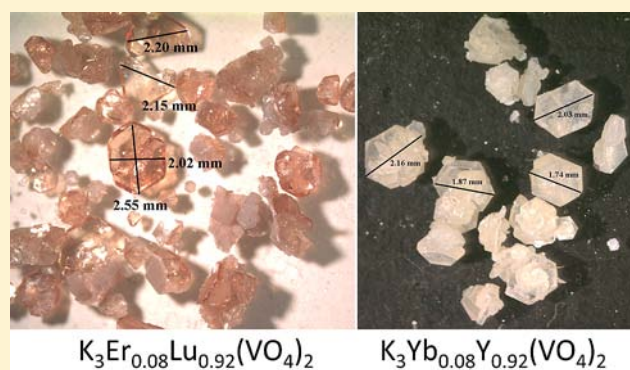
Hydrothermal Synthesis and Spectroscopic Properties of a New Glaserite Material, $K_3RE(VO_4)_2$ (RE = Sc, Y, Dy, Ho, Er, Yb, Lu, or Tm) with Potential Lasing and Optical Properties

Martin M. Kimani, Lindsey Thompson, Whitney Snider, Colin D. McMillen, and Joseph W. Kolis*

Department of Chemistry and Center for Optical Materials Science and Engineering Technologies (COMSET), Clemson University, Clemson, South Carolina 29634-0973, United States

Supporting Information

ABSTRACT: A new series of materials of the glaserite family with the general formula $K_3RE(VO_4)_2$ (RE = Sc, Y, Dy, Ho, Er, Tm, Yb, and Lu) have been hydrothermally synthesized using 10 M K_2CO_3 at 560 °C and characterized by single crystal X-ray diffraction (XRD), powder XRD, differential thermal analysis/thermogravimetric analysis (DTA/TGA), energy-dispersion X-ray (EDX), Raman, infrared, and absorption spectroscopy. All the compounds crystallize in the trigonal $P\bar{3}m1$ space group (No. 164), and their structures contain VO_4 tetrahedra, REO_6 octahedra, and two different $K(1)O_{10}$ and $K(2)O_{12}$ polyhedra. The spectroscopic properties of Nd^{3+} , Yb^{3+} , or Er^{3+} doped $K_3RE(VO_4)_2$ (RE = Y or Lu) are also reported, and the results obtained show that these compounds have promising potential as new laser host materials.



1. INTRODUCTION

Double phosphates, vanadates, molybdates, and tungstates containing transition metals or rare earths with the general formula $(M, M')_4(M''O_4)_2$, where M = alkali metal, M' = Al, In, Cr, Bi, Fe, Sc, Y, RE (rare earths), and M'' = P, V, Mo or W, exhibit interesting structural and chemical properties.¹ Previously published reports show that metal molybdates, tungstates, and selenates such K_2MoO_4 , K_2WO_4 , and $K_3Na(SeO_4)_2$ exhibit ferroelectric, ferroelastic properties.^{2,3} On the other hand double phosphates of rare earths hold considerable promise for use as laser and luminescent materials,^{4–7} while materials such as $K_3Ce(PO_4)_2$ are applicable for ultrafast gamma-ray scintillators because of their high yield and rapid decay times.⁸

The aforementioned compounds are members of an extensive and fascinating class of structures known as the glaserite phases, with the parent derivative having the formula $K_3Na(SO_4)_2$.⁹ Glaserite or apthitalite is a form of anhydrous sulfate ($(K,Na)_3Na(SO_4)_2$) found in the fumaroles of volcanoes.¹⁰ This glaserite structure and its many derivatives are also common in compounds containing silicates, phosphates, molybdates, and tungstates with the general formula A_2XO_4 (where A = Alkali or alkaline earth).^{11–13} The glaserite class family with chemical formula of $A_3B(EX_4)_2$ (where A, B = Li, Na, K, Rb, Cs, NH_4 ; EX_4 = SO_4 , SeO_4 , CrO_4 , WO_4 , RuO_4 , BeF_4 , MoO_4),^{9,10,14–17} are found in different space groups ranging from trigonal, orthorhombic, to monoclinic space groups, often depending on the size of the ions involved. The ideal glaserite structure type crystallizes in the trigonal

space group $P\bar{3}m1$, but most of these compounds exhibit phase transitions from a high temperature phase to a low temperature phase which typically has lower symmetry than the ideal trigonal structure.^{18–20}

Single crystals of glaserite compounds bearing the general formula $A_3RE(VO_4)_2$ (A = alkali metal, RE = Sc, Y, La–Lu) are quite rare, and only a few have been reported to date. These previously reported vanadate containing glaserite compounds include $Na_3Ln(VO_4)_2$ (Ln = La, Nd, and Er), and all have been grown via the flux method and adopt the monoclinic or orthorhombic space groups.^{21–23} In this paper we describe the first hydrothermal growth and crystal structures of glaserite type double vanadate compounds with the general formula $K_3RE(VO_4)_2$ (Ln = Sc, Y, Dy, Ho, Er, Tm, Yb, Lu) adopting the trigonal $P\bar{3}m1$ space group. Raman, infrared, and UV–vis–NIR absorption spectroscopies for most of these glaserite compounds are presented and discussed in detail. The absorption spectra of Er, Nd, or Yb doped $K_3Y(VO_4)_2$ and Er or Yb doped $K_3Lu(VO_4)_2$ are also reported, and the dopant concentrations in the hydrothermally grown crystals were verified using energy-dispersion X-ray spectroscopy (EDX) measurements. The thermal stability of $K_3Y(VO_4)_2$ has been characterized using differential thermal analysis/thermogravimetric analysis (DTA/TGA).

Received: September 3, 2012

Published: December 3, 2012

2. EXPERIMENTAL SECTION

2.1. Synthesis of $K_3RE(VO_4)_2$ (RE = Y, Sc, Dy, Ho, Lu, Tm, Er, or Yb). *Materials.* All reagents were of analytical grade and used as purchased. Several synthetic methods were employed over the course of this study using the following reagents: V_2O_5 (Alfa Aesar, 99.6%), Y_2O_3 (Alfa Aesar, 99.9%), Sc_2O_3 (Strem, 99.9%), Dy_2O_3 (Strem, 99.9%), Ho_2O_3 (Strem, 99.9%), Yb_2O_3 (Strem, 99.9%), Lu_2O_3 (Strem, 99.9%), and Tm_2O_3 (Strem, 99.9%), KVO_3 ((Alfa Aesar, 99.9%), KO_2 (Strem, 99.9%).

Method 1. These compounds were prepared hydrothermally and obtained as phase pure products in the hydrothermal reaction of $REVO_4$ (RE = Y, Sc, Dy, Ho, Lu, Tm, Yb) powders with high concentrations of potassium carbonate mineralizer. The vanadate starting materials $REVO_4$ were first synthesized by stoichiometric solid-state reactions between V_2O_5 with RE_2O_3 at 900 °C for 9 h. As a typical example the synthesis of $K_3Ho(VO_4)_2$ was accomplished via hydrothermal crystallization of ~160 mg of $HoVO_4$ using 0.4 mL of 4–10 M K_2CO_3 at 560 °C in a silver ampule for 6 days. The sealed ampule was loaded into a Tuttle autoclave, which was counter pressured with additional water. The autoclave was heated at 560 °C for 6 days typically generating a counter pressure of 25200 psi. The contents of the ampule were filtered and the products washed with deionized water to yield phase pure crystals as hexagonal plates up to 1 mm in size and 0.5 mm in thickness. The other analogues can be prepared in similar fashion.

Method 2. Phase pure powders of the target glaserite compounds with the general formula $K_3RE(VO_4)_2$ (RE = Y, Sc, Dy, Ho, Lu, Tm, Er, or Yb) were first prepared by solid state reactions of KO_2 , KVO_3 , and RE_2O_3 , respectively, in a molar ratio of 1:2:1 in platinum crucibles air at 1000 °C for 48 h. Hydrothermal recrystallization of ~200 mg of $K_3RE(VO_4)_2$ (prepared from the solid-state reactions described above) using 0.4 mL of 10 M K_2CO_3 at 560 °C in a silver ampule for 6 days afforded the target glaserite products. Crystals prepared by this method were also hexagonal plates, this time up to 2.5 mm in size and 1 mm in thickness.

Method 3. These glaserite compounds can also be synthesized via a KCl/KF flux method. As a typical example the synthesis of $K_3Y(VO_4)_2$ was accomplished by heating a mixture of Y_2O_3 , V_2O_5 , KF, and KCl in a molar ratio of 1:1:5:8 in platinum crucibles under air at 1000 °C for 24 h. The temperature was slowly cooled at a rate of 5 °C/h from 1000 to 500 °C, and then the furnace was turned off and the sample was cooled to room temperature over the next 5 h. The crystals obtained with this method are typically platelets 0.05 mm thick with diameters of 2 mm.

Rare Earth Doped $K_3Y(VO_4)_2$ and $K_3Lu(VO_4)_2$. Yttrium- and lutetium-based glaserites were identified as potentially interesting host materials. Rare earth doped crystals for spectroscopic characterizations were typically prepared based on Method 2 above. Powders of the doped glaserite compounds (Rare Earth dopants = Nd (3, 5, 8, 10, and 15%); Yb or Er (3, 5, and 8%)) were prepared by solid state reactions of KO_2 , KVO_3 , and $RE:Y_2O_3$ (RE = Nd, Yb, or Er) in a molar ratio of 1:2:1, respectively, in platinum crucibles in air at 1000 °C for 48 h. The doped yttrium oxide or lutetium oxide precursors were first synthesized via a coprecipitation procedure where, for example, a mixture of Y_2O_3 with the appropriate amount of the desired dopant (as RE_2O_3) was dissolved in 40 mL of deionized water and 10 mL of 18 M HNO_3 . The reaction mixture was stirred on a hot plate at a temperature of 80 °C until all the contents were fully dissolved. The dissolved contents were left to cool down to room temperature and to this was added 100 mL of deionized water. This acidic solution was titrated with 300 mL of 15% NH_4OH resulting in the formation of a precipitate. The precipitate was filtered, rewashed twice with deionized water, and oven-dried at 120 °C for 2 h and at 1000 °C for 24 h. Hydrothermal recrystallization of the doped powders obtained from the solid state reaction using 10 M K_2CO_3 at 560 °C in a silver ampule for 6 days afforded the target doped-glaserite crystals. Additional phases ($NdO(OH)$) were segregated during the hydrothermal growth when the Nd^{3+} doping concentration exceeded 10%.

2.2. X-ray Diffraction. Powder X-ray diffraction was used to characterize the bulk solids, and single crystal X-ray diffraction was used to identify and structurally characterize the new glaserite species. Powder X-ray diffraction (PXRD) data was collected using a Rigaku Ultima IV X-ray diffractometer with $Cu K\alpha$ radiation ($\lambda = 1.5418 \text{ \AA}$). Patterns were collected from 5 to 90 degrees in 2θ at a scan speed of 1.0 deg/min. All single crystal XRD solutions were confirmed using PXRD data and compared to predicted powder patterns simulated from the single crystal data using the Mercury program.²⁴ Single crystal X-ray intensity data were collected using a Mercury CCD detector and a Rigaku AFC8S diffractometer equipped with a graphite monochromated $Mo K\alpha$ radiation ($\lambda = 0.71073 \text{ \AA}$). The space groups were determined from the observed systematic absences and confirmed using the MISSYM algorithm within the PLATON program suite.²⁵ Data reduction, application of Lorentz and polarization effects and absorption corrections were performed using the CrystalClear program.²⁶ The structures were solved by direct methods and refined using subsequent Fourier difference techniques, by full-matrix least-squares, on F^2 using SHELXTL 6.10.²⁷ All atoms were refined anisotropically. All single crystal solutions were confirmed by simulating the powder pattern from the single crystal structure determinations and comparing these to the powder patterns obtained from the bulk reaction products.

2.3. Spectroscopy and Other Characterization. Infrared spectroscopy was performed using the KBr pellet technique under flowing nitrogen with a Nicolet Magna 550 IR spectrometer. Spectra obtained were the average of 16 scans over a 400–4000 cm^{-1} range with 4 cm^{-1} resolution. UV–vis–NIR absorption spectra of the glaserite compounds were also conducted using glaserite samples blended in KBr pellets. These spectra were obtained using a Perkin-Elmer Lambda 900 UV/vis/near-IR spectrometer in the scanning range of 190 to 2100 nm using 4 nm/sec scan speed.

An Ar laser (Innova 200, Coherent) operating at 514.5 nm and 18 mW at the sample was employed for excitation of Raman scattering. The scattered light was collected by an $f/1.2$ camera lens in a 1808 backscattering geometry and analyzed by a triple spectrometer (Tripletmate 1877, Spex) equipped with a charge-coupled device (CCD) detector (iDUS 420 series, Andor) cooled to –60 °C. Typical spectra acquisition time was 10 s. The Raman spectrum of indine was used for spectral calibration. A glass capillary holder was fabricated for suspending the polycrystalline glaserite compounds, in such a way that the plane of the substrate was normal to the collection optics.

The DSC/TGA experiment was performed on a SDT Q600 (V20.9 Build 20) instrument. The sample was put into an alumina crucible and was heated in a nitrogen atmosphere at 10 °C/min from room temperature to a final temperature of 1400 °C.

EDX measurements were performed using a Bruker Quantax 70 EDX analyzer attached to a Hitachi TM-3000 scanning electron microscope. Average dopant concentrations for each crystal were obtained using an accelerating voltage of 15 kV at multiple analysis points measured against a copper standard. All the EDX spectra showed simultaneous presence of potassium, yttrium, vanadium, oxygen, and the respective lanthanide dopant ion peaks. Concentration is reported in atomic percent relative to the host metal site (for example 5% Nd: $K_3Y(VO_4)_2$ represents a composition of $K_3Nd_{0.05}Y_{0.95}(VO_4)_2$).

3. RESULTS AND DISCUSSION

3.1. Synthesis and Structure of Trigonal Glaserites with General Formula $K_3RE(VO_4)_2$ (RE = Sc, Y, Dy, Er, Ho, Tm, Yb, Lu). This work was initially prompted by our earlier hydrothermal growth studies of YVO_4 single crystals. During our earlier and subsequent detailed crystal growth study,^{28,29} we noticed that the use of lower concentrations of K_2CO_3 mineralizers (2–4 M) resulted in growth of bulk YVO_4 crystals and other interesting V^{4+} minor products with the formula $Y_3VO_5(OH)_3$ or $Y_2O(VO_4)$.²⁸ Interestingly, when higher concentration of carbonates are used as mineralizers (≥ 4 M

K_2CO_3) an entirely different phase pure material is obtained with the formula $\text{K}_3\text{Y}(\text{VO}_4)_2$ (Figure 1) which forms at the

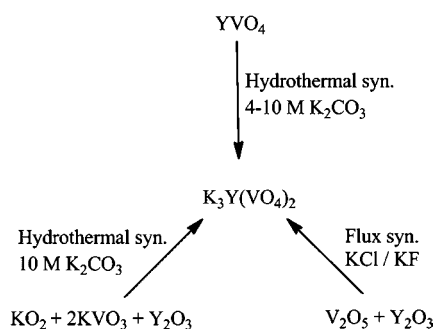


Figure 1. Reaction scheme showing the synthesis of the glaserite vanadate material $\text{K}_3\text{Y}(\text{VO}_4)_2$ based on synthetic methods 1–3.

expense of the parent YVO_4 . In this case the compounds contain exclusively V^{5+} vanadate building blocks with no reduced V^{4+} or V^{3+} evident, as demonstrated by the colorless nature of the crystals. This phase was likely stabilized by the higher concentration of K_2CO_3 employed since additional K^+ ions were available for reaction with the YVO_4 feedstock.

Further work on our part demonstrated that the target products can also be prepared by solid state reactions of KO_2 , KVO_3 , and A_2O_3 ($\text{A} = \text{Y}, \text{Sc}, \text{Dy}, \text{Ho}, \text{Lu}, \text{Tm}, \text{Yb}$), respectively, in a molar ratio of 1:2:1 in platinum crucibles in air at 1000 °C for 48 h. The obtained powders could then be hydrothermally recrystallized with 10 M K_2CO_3 at 560 °C in a silver ampule for 6 days to afford the target glaserite products. Glaserite compounds synthesized using synthetic method 2, were of better quality and thickness compared to those synthesized using methods 1 and 3. Attempts to grow other glaserite compounds with larger lanthanide atoms such as La–Tb were unsuccessful and resulted in the formation of $\text{LnO}(\text{OH})$ and LnVO_4 (where $\text{Ln} = \text{La}–\text{Tb}$). Chemically speaking, Dy appears to act as the boundary for the glaserite phase formation in hydrothermal fluids because of the stability of these other phases. Glaserites based on Ga or Al were not obtained, and only the oxyhydroxide products were identified, so there is

likely a similar boundary to the phase stability in terms of how small of a trivalent ion will be supported. All the glaserite compounds synthesized are air stable and nonhygroscopic.

EDX measurements were employed to analyze the composition of the Ln^{3+} doped $\text{K}_3\text{Y}(\text{VO}_4)_2$ and $\text{K}_3\text{Lu}(\text{VO}_4)_2$ ($\text{Ln} = \text{Nd}, \text{Er}, \text{Yb}$) crystals after hydrothermal treatment (Supporting Information, Figure SI 1). Of particular interest is identifying the degree of observed dopant segregation into the $\text{LnO}(\text{OH})$ phases to accurately characterize the dopant concentration in the as-grown crystals (Table 1). EDX results on the $\text{Nd}:\text{K}_3\text{Y}(\text{VO}_4)_2$ revealed that the measured dopant concentrations in the hydrothermally grown crystals were about 10–15% lower than those found in the feedstock used to grow them. There appears to be a greater partition coefficient between the Y^{3+} host and Nd^{3+} dopant ions in this hydrothermal system than Er^{3+} or Yb^{3+} dopant ions, likely owing to the better size match between Y^{3+} and the smaller lanthanide ions, or simply indicating a greater stability for $\text{NdO}(\text{OH})$ crystallized from the hydrothermal fluid. Even so, the partition coefficient appears similar for all Nd^{3+} concentrations and high dopant concentrations can be achieved for all of the dopants studied. In the case of the $\text{K}_3\text{Lu}(\text{VO}_4)_2$ host, about 10–15% of Er^{3+} or Yb^{3+} dopant is lost upon hydrothermal crystallization. While this was anticipated in the case of $\text{Er}:\text{K}_3\text{Lu}(\text{VO}_4)_2$, we are somewhat surprised that the better size match between Lu^{3+} and Yb^{3+} did not lead to less (or comparable) dopant partitioning than in $\text{Yb}:\text{K}_3\text{Y}(\text{VO}_4)_2$.

Data from the single crystal structure refinements of newly synthesized glaserite compounds are given in Tables 2 and 3. The hydrothermally grown glaserite crystals in this study all exhibit trigonal symmetry, crystallizing in space group $P\bar{3}m1$ (no. 164). The structures could be solved in the monoclinic space group $C2/c$ (no. 15), but in all cases searches for higher symmetry indicated the presence of trigonal symmetry. Likewise, determining the structure in space group $P\bar{1}$ also resulted in a recommended transformation to space group $P\bar{3}m1$ rather than space group $C2/c$ which was previously proposed for $\text{K}_3\text{Y}(\text{VO}_4)_2$ (PDF No: 00-049-1227) based on a Rietveld refinement on a powder prepared by solid state techniques.³⁰ The trigonal space group $P\bar{3}m1$ for $\text{K}_3\text{RE}(\text{VO}_4)_2$ ($\text{RE} = \text{Y}, \text{Sc}, \text{Dy}, \text{Ho}, \text{Lu}, \text{Tm}, \text{Er}, \text{or Yb}$) compounds obtained

Table 1. Elemental Analysis of Dopant Concentration in Feedstock and Hydrothermally Grown Glaserite Crystals

host compound	dopant ion	dopant concentration in feedstock (at. %)	dopant concentration in hydrothermally grown crystals (at. %)	percentage of initial dopant in hydrothermally grown crystals
$\text{K}_3\text{Y}(\text{VO}_4)_2$	Nd^{3+}	15.0	13.5	90
$\text{K}_3\text{Y}(\text{VO}_4)_2$	Nd^{3+}	10.0	8.4	84
$\text{K}_3\text{Y}(\text{VO}_4)_2$	Nd^{3+}	8.0	6.9	86
$\text{K}_3\text{Y}(\text{VO}_4)_2$	Nd^{3+}	5.0	4.2	84
$\text{K}_3\text{Y}(\text{VO}_4)_2$	Nd^{3+}	3.0	2.8	93
$\text{K}_3\text{Y}(\text{VO}_4)_2$	Er^{3+}	8.0	7.8	98
$\text{K}_3\text{Y}(\text{VO}_4)_2$	Er^{3+}	5.0	4.7	94
$\text{K}_3\text{Y}(\text{VO}_4)_2$	Er^{3+}	3.0	2.9	97
$\text{K}_3\text{Y}(\text{VO}_4)_2$	Yb^{3+}	8.0	7.9	99
$\text{K}_3\text{Y}(\text{VO}_4)_2$	Yb^{3+}	5.0	4.8	96
$\text{K}_3\text{Y}(\text{VO}_4)_2$	Yb^{3+}	3.0	3.0	100
$\text{K}_3\text{Lu}(\text{VO}_4)_2$	Er^{3+}	8.0	6.9	86
$\text{K}_3\text{Lu}(\text{VO}_4)_2$	Er^{3+}	5.0	4.2	84
$\text{K}_3\text{Lu}(\text{VO}_4)_2$	Er^{3+}	3.0	2.7	90
$\text{K}_3\text{Lu}(\text{VO}_4)_2$	Yb^{3+}	8.0	7.2	90
$\text{K}_3\text{Lu}(\text{VO}_4)_2$	Yb^{3+}	5.0	4.1	82
$\text{K}_3\text{Lu}(\text{VO}_4)_2$	Yb^{3+}	3.0	2.8	93

Table 2. Crystallographic Data for Newly Reported Glaserite Compounds

	1	2	3	4
chemical formula	K ₃ YV ₂ O ₈	K ₃ DyV ₂ O ₈	K ₃ HoV ₂ O ₈	K ₃ LuV ₂ O ₈
F.W. (g/mol)	436.09	509.68	512.11	522.15
space group	<i>P</i> $\bar{3}$ <i>m</i> 1	<i>P</i> $\bar{3}$ <i>m</i> 1	<i>P</i> $\bar{3}$ <i>m</i> 1	<i>P</i> $\bar{3}$ <i>m</i> 1
temp./K	293	293	293	293
crystal system	trigonal	trigonal	trigonal	trigonal
<i>a</i> , Å	5.8889(8)	5.9016(8)	5.8495(8)	5.855(2)
<i>b</i> , Å	5.8889(8)	5.9016(8)	5.8495(8)	5.855(2)
<i>c</i> , Å	7.6295(15)	7.6047(15)	7.5737(15)	7.578(3)
α , deg	90	90	90	90
β , deg	90	90	90	90
γ , deg	120	120	120	120
<i>V</i> , Å ³	229.14(6)	229.38(6)	224.43(6)	225.01(1)
<i>Z</i>	1	1	1	1
<i>D</i> _{calc} , Mg/m ³	3.160	3.690	3.789	3.853
indices (min)	[-8, -8, -8]	[-6, -7, -9]	[-6, -7, -8]	[-7, -7, -8]
(max)	[8, 7, 10]	[7, 7, 9]	[7, 6, 9]	[7, 7, 9]
parameters	21	21	21	20
<i>F</i> (000)	206	233	234	238
μ , mm ⁻¹	9.649	11.427	12.169	14.315
2 θ range, deg	2.67 to 30.19	2.68 to 29.27	2.69 to 26.91	2.69 to 25.57
collected reflections	2363	2117	1684	1977
unique reflections	271	239	208	192
final <i>R</i> (obs. data), ^a <i>R</i> ₁	0.0381	0.0403	0.0308	0.0234
<i>wR</i> ₂	0.0942	0.1059	0.0521	0.0587
final <i>R</i> (all data), <i>R</i> ₁	0.0381	0.0403	0.0359	0.0234
<i>wR</i> ₂	0.0942	0.1059	0.0570	0.0587
goodness of fit (<i>S</i>)	1.143	1.189	1.190	1.398
extinction coefficient	0.065(11)	0.032(9)	0.094(8)	

$${}^a R_1 = \frac{\sum |F_o| - |F_c|}{\sum |F_o|}; wR_2 = \left\{ \frac{\sum w[(F_o)^2 - (F_c)^2]^2}{\sum w(F_o)^2} \right\}^{1/2}.$$

from single crystal determinations was further verified via PXRD analysis, and patterns of the as-synthesized crystals were compared to those simulated from the single crystal structure determinations. These are shown in Figure 2.

The experimental pattern appears to be a better match for the pattern simulated from the trigonal crystal data, and does not contain a number of the peaks exhibited by the more complicated pattern based on the lower symmetry monoclinic data (and those peaks indexed in PDF 00-049-1227). Thus it appears clear that the hydrothermally grown crystals are all trigonal in their symmetry. We also note from the powder data that the target glaserite phase is the primary product obtained, with only a few minor peaks assigned to a trace impurity phase. The minor impurity phase has been assigned to YVO₄ residue formed during the solid state synthesis of K₃Y(VO₄)₂, which is easily recrystallized hydrothermally. Powder patterns for the other rare earth analogues, K₃RE(VO₄)₂ (RE = Sc, Lu, Er, Ho, Tm, and Yb) are given in Supporting Information Figures SI 2 to SI 7.

The crystal structures of K₃RE(VO₄)₂ (RE = Sc, Y, Dy, Er, Ho, Tm, Yb, Lu) are members of an extensive and fascinating class of structures known as the glaserite phases, with the

Table 3. Crystallographic Data for Newly Reported Glaserite Compounds

	5	6	7	8
chemical formula	K ₃ TmV ₂ O ₈	K ₃ YbV ₂ O ₈	K ₃ ScV ₂ O ₈	K ₃ ErV ₂ O ₈
F.W. (g/mol)	516.11	520.22	392.14	514.44
space group	<i>P</i> $\bar{3}$ <i>m</i> 1			
temp./K	293	293	293	293
crystal system	trigonal	trigonal	trigonal	trigonal
<i>a</i> , Å	5.8835 (8)	5.8453(8)	5.7638(8)	5.8798(8)
<i>b</i> , Å	5.8835(8)	5.8453(8)	5.7638(8)	5.8798(8)
<i>c</i> , Å	7.6085 (15)	7.5694(15)	7.4746(15)	7.6035(15)
α , deg	90	90	90	90
β , deg	90	90	90	90
γ , deg	120	120	120	120
<i>V</i> , Å ³	228.09(6)	223.98(6)	215.05(6)	227.65(6)
<i>Z</i>	1	1	1	1
<i>D</i> _{calc} , Mg/m ³	3.757	3.857	3.028	3.752
indices (min)	[-7, -8, -10]	[-7, -7, -9]	[-7, -7, -10]	[-7, -7, -9]
(max)	[7, 8, 8]	[7, 7, 8]	[7, 7, 9]	[7, 7, 9]
parameters	20	21	20	20
<i>F</i> (000)	236	237	188	235
μ , mm ⁻¹	13.026	13.800	4.357	12.524
2 θ range, deg	4.00 to 29.62	2.69 to 29.58	2.73 to 29.89	2.68 to 27.64
collected reflections	2302	2208	2221	2093
unique reflections	260	252	239	231
final <i>R</i> (obs. data), ^a <i>R</i> ₁	0.0345	0.0331	0.0291	0.0228
<i>wR</i> ₂	0.0822	0.0749	0.0739	0.0510
final <i>R</i> (all data), <i>R</i> ₁	0.0354	0.0332	0.0296	0.0228
<i>wR</i> ₂	0.0831	0.0749	0.0743	0.0510
goodness of fit (<i>S</i>)	1.224	1.169	1.254	1.156
extinction coefficient		0.019(4)		

$${}^a R_1 = \frac{\sum |F_o| - |F_c|}{\sum |F_o|}; wR_2 = \left\{ \frac{\sum w[(F_o)^2 - (F_c)^2]^2}{\sum w(F_o)^2} \right\}^{1/2}.$$

parent derivative having the formula K₃Na(SO₄)₂.⁹ All the newly reported compounds crystallize in the trigonal space-group *P* $\bar{3}$ *m*1 (No. 164). The atoms Y(1) and K(2) sit on special positions with site symmetry $\bar{3}m$, while atoms V(1), O(2), and K(1) have site symmetry $3m$ and atom O(1) has site symmetry m . The structures are made up of VO₄ tetrahedra, REO₆ octahedra and two different K(1)O₁₀ and K(2)O₁₂ polyhedra. The crystal structure of K₃Y(VO₄)₂ contains an octahedrally coordinated Y³⁺ cation with symmetry related Y–O bond distances of 2.224 (5) Å. The V⁵⁺ cation adopts a tetrahedral geometry with O–V–O angles of 109.5 and three equal and one shorter V–O bonds of 1.712 (6) and 1.603 (10) Å, respectively (Figure 3 and Table 4).

The K(1) cation in K₃Y(VO₄)₂ adopts a ten-coordinate geometry (Figure 4A) with K–O interatomic distances ranging from 2.552 (10) to 3.320 (9) Å, whereas the K(2) cation contains a 12-coordinate geometry (Figure 4B) with K–O interatomic distances ranging from 3.065 (9) to 3.415 (10) Å. The average K–O interatomic distances in K(1)O₁₀ and K(2)O₁₂ polyhedra in K₃Y(VO₄)₂ are 3.025(9) Å and 3.240 (5) Å, respectively, and these are slightly longer compared to the average K–O bond distances of KO₁₀ and KO₁₂ polyhedra in other reported glaserite compounds such as K₃Na(SO₄)₂

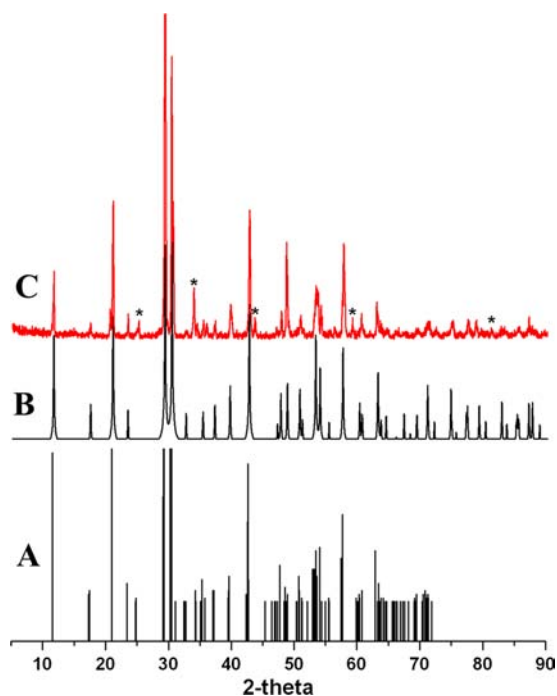


Figure 2. XRD patterns of (A) monoclinic phase $K_3Y(VO_4)_2$ (PDF No:00-049-1227) compared with (B) simulated trigonal phase of $K_3Y(VO_4)_2$ (from present work), and (C) experimental patterns of the newly synthesized trigonal phase of $K_3Y(VO_4)_2$. The asterisk (*) sign denotes impurity peaks due to YVO_4 .

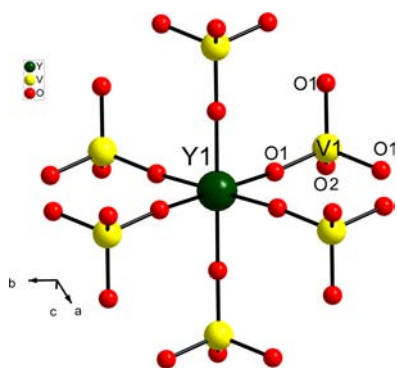


Figure 3. Octahedral and tetrahedral coordination environments around the Y^{3+} and V^{5+} atoms in $K_3Y(VO_4)_2$, respectively.

Table 4. Selected Interatomic Distances for $K_3RE(VO_4)_2$ (RE = Sc, Y, and Lu)

	RE = Sc	RE = Y	RE = Lu
RE(1)–O(1) × 6	2.105 (2)	2.224 (5)	2.188 (7)
V(1)–O(2)	1.637 (4)	1.603 (10)	1.653 (14)
V(1)–O(1) × 3	1.735 (2)	1.712 (6)	1.712 (8)
K(1)–O(2)	2.581 (4)	2.552 (10)	2.502 (15)
K(1)–O(1) × 6	2.8873 (10)	2.9567 (9)	2.9411 (15)
K(1)–O(1) × 3	3.121 (2)	3.320 (9)	3.275 (11)
K(2)–O(1) × 6	3.017 (2)	3.065 (9)	3.061 (11)
K(2)–O(2) × 6	3.3380 (6)	3.415 (10)	3.3916 (17)

(2.893 and 3.103 Å),⁹ $K_3V(VO_4)_2$ (2.947 and 3.133 Å),³¹ $K_3Na(CrO_4)_2$ (2.969 and 3.155 Å),¹⁶ and $K_3Na(RuO_4)_2$ (3.022 and 3.238 Å).¹⁷ Examining the selected interatomic distances in Table 4 for the family of compounds prepared in this study we see that the glaserite structure has a certain amount of flexibility

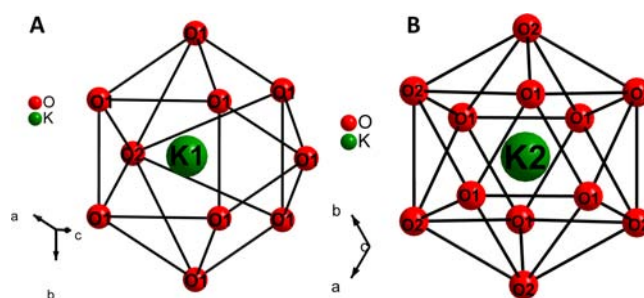


Figure 4. Coordination polyhedra of the crystallographically unique K^+ cations in $K_3Y(VO_4)_2$ structure.

in its framework structure to accommodate the various sizes of rare earth ions explored. We note that the presence of smaller rare earth ions result in lengthening of the V–O bond distances, but a general shortening of the K–O distances (with the exception being the shortest K–O bond, K1–O2, which becomes longer). This occurs because the RE–O bond distance contracts to a greater degree (for example, 5.3% for Sc–O vs Y–O) than the expansion of V–O bond distance (1.2%) in the same compounds.

The extended structure of $K_3Y(VO_4)_2$ is shown in Figure 5, and its crystal chemistry can be described using a pinwheel

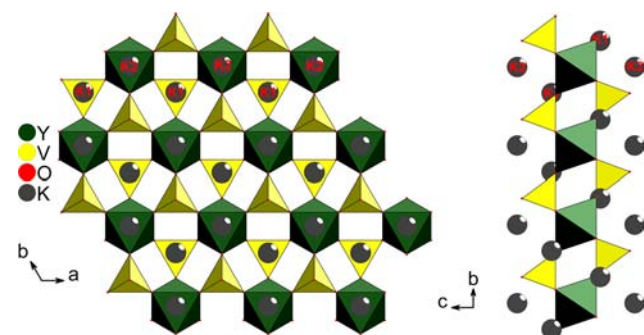


Figure 5. Extended structure of $K_3Y(VO_4)_2$ along the c -axis (left) and a -axis (right).

bracelets model introduced by Moore in the description of glaserite-like sulfate.³² Adopting this approach for the glaserite type double vanadates, the pinwheel subunit is formed by the $[YO_6]$ octahedron that shares its six corners with $[VO_4]^{3-}$ tetrahedra that alternate up and down. The pinwheels are linked through $[VO_4]^{3-}$ tetrahedra to form layers with potassium atoms located between the layers. When viewed along the c -axis the $[VO_4]^{3-}$ tetrahedron is corner shared to three $[YO_6]$ octahedra and edged shared with two $[(K2)O_{12}]$ polyhedra and one $[(K1)O_{10}]$ polyhedron. The $[(K1)O_{10}]$ polyhedron is edge shared by three $[YO_6]$ polyhedra, two $[VO_4]^{3-}$ tetrahedra, and two $[(K2)O_{12}]$ polyhedra, whereas the $[(K2)O_{12}]$ polyhedron edge shares to itself resulting in the formation of those layers. Of particular note is the RE–RE separation distance in the glaserite structure type since there is no RE–O–RE bridging. In all cases the rare earth ions are separated by one edge of a VO_4 tetrahedron resulting in large spacing of rare earth ions: 5.76, 5.89, and 5.86 Å in the Sc, Y and Lu based compounds, respectively. This can have profound effects for the optical behavior and lasing performance upon doping since quenching mechanisms between dopant ions are mitigated by the long rare earth distances. Thus it is possible

that unusually long lifetimes can be observed and higher dopant concentrations can be employed. Studies of these effects in this new class of rare earth glaserites are underway.

3.3. IR Spectroscopy. Infrared spectroscopy was used to probe the coordination geometry of the vanadium cation in the title compounds. The infrared spectra of $K_3RE(VO_4)_2$ ($RE = Y, Yb, Sc, Ho,$ and Dy) showing the areas of interest is displayed in Figure 6 while the entire spectra are shown in Supporting

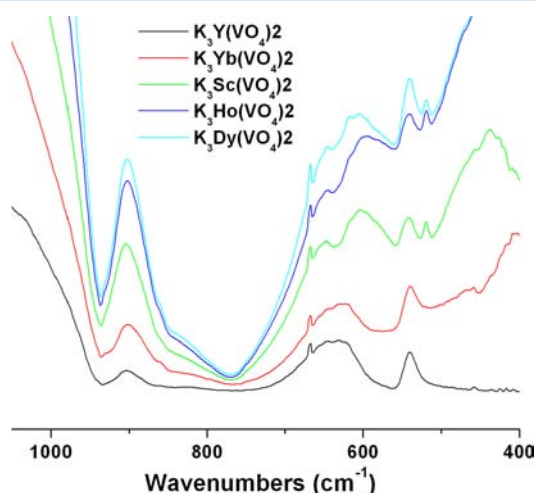


Figure 6. Infrared spectra of $K_3RE(VO_4)_2$ ($RE = Sc, Y, Yb, Ho, Dy$) compounds in KBr. Y-axis units are in % transmittance.

Information, Figure SI 8. The IR spectra of the investigated glaserite compounds $K_3RE(VO_4)_2$ ($RE = Y, Yb, Sc, Ho,$ and Dy) showed absorption bands ranging from 449 to 940 cm^{-1} . In particular the infrared spectrum of $K_3Y(VO_4)_2$ has a weak absorption peak at 465 cm^{-1} , and three other strong absorption bands with peaks centered at 561, 770, and 936 cm^{-1} . The weak absorption band at 465 cm^{-1} corresponds to vibrations of Y–O bonds,^{33–35} while the peak at 561 cm^{-1} is assigned to the bending ν_4 vibrations of VO_4^{3-} subunits.^{36,37} The band at 768 cm^{-1} and 940 cm^{-1} can be attributed to $\nu(V-O)$,³⁸ of the three longer V–O bonds (1.712 (6) Å) and one shorter V–O bond (1.603 (10) Å) found within the VO_4 tetrahedra of the glaserite compound. The short axial V–O bond is blue-shifted relative to the longer equatorial V–O bonds since it is a much stronger bond.

3.4. Raman Spectroscopy. The reported glaserite compounds belong to the space group $P\bar{3}m1 = D_{3d}^3$. The general observed atomic coordinates of $K_3RE(VO_4)_2$ glaserite compound in the $P\bar{3}m1$ space group is shown in Table 5 where $K_3Y(VO_4)_2$ is used as a representative example.

The one molecule of $K_3RE(VO_4)_2$ per primitive cell in the D_{3d}^3 structure supports $3 \times 1 \times 14 = 42$ modes of vibration with

Table 5. Atomic Coordinates of $K_3Y(VO_4)_2$ in a D_{3d}^3 Crystal System

atom	Wyck.	site sym.	x	y	z
Y1	1b	$-3m$	1.00000	0	1/2
V1	2d	$3m$	2/3	1/3	0.74849
O1	6i	m	0.35037	0.17518	0.67351
O2	2d	$3m$	2/3	1/3	0.95866
K1	2d	$3m$	2/3	1/3	1.29314
K2	1a	$-3m$	0	0	1.00000

$K = 0$ including the zero-frequency translational motion of the crystal. These vibrations are classified according to irreducible representations of the point group of the elementary cell.³⁹ The 42 modes of vibration of the full symmetry group of $K_3RE(VO_4)_2$ results into the following irreducible representations of D_{3d}^3 :

$$\Gamma_{42} = 5A_{1g} + A_{1u} + A_{2g} + 7A_{2u} + 6E_g + 8E_u$$

For each VO_4^{3-} molecular ion, nine internal Raman vibration modes are expected from the general formula $3n - 6$. The VO_4^{3-} anions in the reported glaserite molecules adopt C_{3v} point group, and their internal vibrations can be described by the following representation, where $3A_{1g} + 3E_g$ represent the Raman active modes while $3A_{2u} + 3E_u$ represent the IR active modes:

$$3A_{1g} + 3A_{2u} + 3E_g + 3E_u$$

The observed internal Raman vibrations from VO_4^{3-} ion in C_{3v} symmetry can be well understood when compared to the free VO_4^{3-} ion in tetrahedral symmetry. The free VO_4^{3-} ion is tetrahedral (T_d point group) and its irreducible representation can be presented as

$$\Gamma_{\text{isolated } VO_4} = A_1(R) + E(R) + 2F_2(R, IR)$$

The A_1 mode is the symmetric stretching ν_1 (Raman active, 878 cm^{-1}), while the E mode is the symmetric bending ν_2 (Raman active, 345 cm^{-1}). The two F_2 modes correspond to the asymmetric stretching ν_3 (Raman and infrared active, 825 cm^{-1}), and the asymmetric deformation ν_4 (Raman and infrared active, 480 cm^{-1}).^{40–42} In the reported glaserite compounds, one oxygen atom is bonded to V with a shorter bond than the other three so the symmetry is lowered to C_{3v} relative to the free VO_4^{3-} ion which adopts T_d symmetry. Thus the two F_2 modes observed in free tetrahedral VO_4^{3-} ions are split into $A_1 + E$ modes for the VO_4^{3-} ions in C_{3v} symmetry in $K_3RE(VO_4)_2$ compounds. Hence when the T_d symmetry is lowered to C_{3v} , the irreducible representation changes to the following:

$$\Gamma_{C_{3v} VO_4} = 3A_1 + 3E$$

Under the factor group D_{3d}^3 each $3A_1$ mode gives rise to $3A_{1g}$ (R) + $3A_{2u}$ (IR) modes while $3E$ mode gives rise to $3E_g$ (R) + $3E_u$ (IR) modes (Table 6; where R and IR refers to Raman and infrared modes).

Table 6. Reduction of VO_4^{3-} Modes from T_d to C_{3v} in a D_{3d}^3 crystal

free T_d	C_{3v}	D_{3d}^3
A_1	$3A_1$	$3A_{1g}$ Raman
E	$3E$	$3A_{2u}$ IR $3E_g$ Raman
$2F_2$	$3E$	$3E_u$ IR

We present the Raman spectra of $K_3RE(VO_4)_2$ in Figure 7 and the Supporting Information, Figure SI 9 showing the internal and external vibrational modes detected. These newly synthesized glaserite materials show internal vibrational modes, with the peak in the range of 932–946 cm^{-1} corresponding to the symmetric stretching ν_1 . This ν_1 stretching vibration in

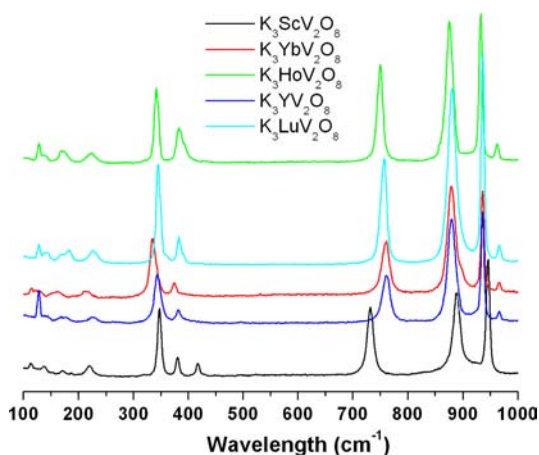


Figure 7. Raman spectra of glaserite compounds in the range of 100–1000 cm^{-1} .

isolated orthovanadate ions is expected and reported to correspond to the strongest Raman peak. The peaks in the range of 732–762 cm^{-1} and 875–888 cm^{-1} most likely correspond to the ν_3 asymmetric stretching mode, whereas the peaks in the range of 374–395 cm^{-1} and 334–349 cm^{-1} have been assigned to ν_4 asymmetric deformation and ν_2 symmetric bending modes, respectively (Table 7). In the external

Table 7. Internal Raman Mode Frequencies of VO_4^{3-} Anion in the Glaserite Compounds Compared to YVO_4 and Free VO_4^{3-} Anion

crystal	ν_1	ν_3	ν_3	ν_4	ν_2
$\text{K}_3\text{Sc}(\text{VO}_4)_2$	946	888	732	380	349
$\text{K}_3\text{Y}(\text{VO}_4)_2$	936	880	762	383	343
$\text{K}_3\text{Yb}(\text{VO}_4)_2$	937	879	761	374	334
$\text{K}_3\text{Er}(\text{VO}_4)_2$	932	876	752	383	343
$\text{K}_3\text{Lu}(\text{VO}_4)_2$	937	880	758	383	345
$\text{K}_3\text{Ho}(\text{VO}_4)_2$	932	875	751	395	341
YVO_4	891	840	817	395	260
Free VO_4^{3-}	878	825		480	345

vibrational modes five peaks are observed in the range of 100–250 cm^{-1} . These bands below 250 cm^{-1} are complicated and may be attributed to K–O bonds and lattice vibrations.⁴³

3.5. DTA/TGA Analysis. The thermal stability of $\text{K}_3\text{Y}(\text{VO}_4)_2$ crystals was investigated by heating the crystals in a thermal range of 100–1300 °C in a nitrogen flowing atmosphere. The entire heat treatment comprises one endothermic process as seen from the DTA curve (Figure 8). The results indicated that upon heating the glaserite $\text{K}_3\text{Y}(\text{VO}_4)_2$ melts at 1150 °C and undergoes decomposition at temperatures above 1250 °C. The heat treatment process is also accompanied by a small, gradual mass loss as depicted on the TGA curve (Figure 8). Previous results by Bobylev et al. determined that the glaserite compound $\text{K}_3\text{Y}(\text{VO}_4)_2$ (monoclinic phase) is composed of a pseudobinary system containing YVO_4 – K_3VO_4 , which undergoes weight loss upon heating.³⁰ The weight loss observed upon heating $\text{K}_3\text{Y}(\text{VO}_4)_2$ is attributed to the evaporation of potassium orthovanadate, and the decomposition process might proceed according to the proposed scheme below:

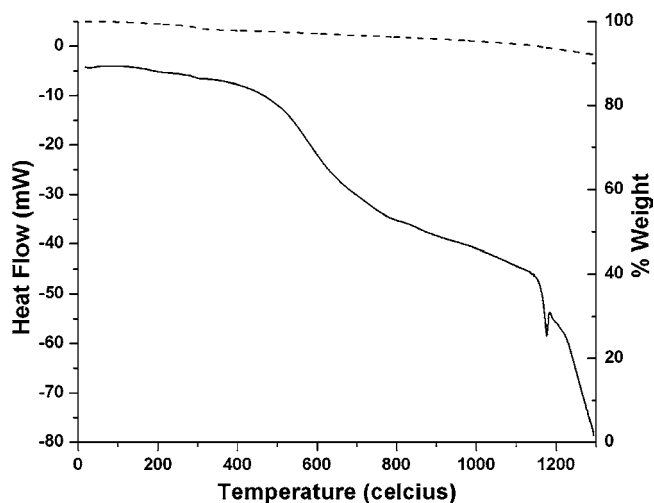
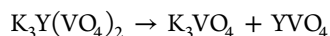


Figure 8. DTA (solid line) and TGA (dotted line) curves of $\text{K}_3\text{Y}(\text{VO}_4)_2$ in a nitrogen atmosphere.

3.6. Optical Characterization of Rare Earth Glaserites.

The absorption spectra of the newly synthesized glaserite compound $\text{K}_3\text{Er}(\text{VO}_4)_2$ is shown in Figure 9 while the rest are

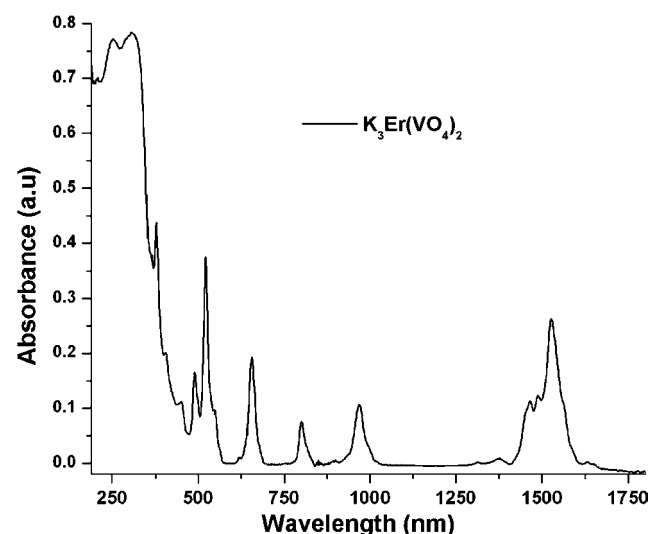


Figure 9. Absorption spectrum of $\text{K}_3\text{Er}(\text{VO}_4)_2$.

shown in the Supporting Information Figures SI 10 and SI 11. All the compounds exhibit a distinct band centered at ~ 320 nm which corresponds to the charge transfer band of oxygen to vanadium(V).^{44,45} The region 200 to 400 nm is usually attributed to the presence of V^{5+} tetrahedrally coordinated VO_4 species.^{46,47} The spectrum of $\text{K}_3\text{Yb}(\text{VO}_4)_2$ also depicts a broad absorption band from 900 to 1060 nm, and the strongest peak is located at about 970 nm which correspond to ${}^2\text{F}_{7/2}$ to ${}^2\text{F}_{5/2}$ transition in Yb^{3+} .⁴⁸ The dysprosium containing glaserite $\text{K}_3\text{Dy}(\text{VO}_4)_2$ shows the expected transitions for Dy^{3+} ion in the near IR region with the sharpest peak centered around 1273, 1094, 895, 800, and 752 nm corresponding to (${}^6\text{F}_{11/2} + {}^6\text{H}_{9/2}$), (${}^6\text{F}_{9/2} + {}^6\text{H}_{7/2}$), ${}^6\text{F}_{7/2}$, ${}^6\text{F}_{5/2}$ and ${}^6\text{F}_{3/2}$ transitions from the ground state, respectively.^{49–51} The absorption spectra of $\text{K}_3\text{Er}(\text{VO}_4)_2$ (Figure 9) shows the following absorption peaks: 1527, 967, 798, 655, 521, 488, 449, 408, and 377 nm which correspond to 4f-f transitions from the ground state ${}^4\text{I}_{15/2}$ to

$^4I_{13/2}$, $^4I_{11/2}$, $^4I_{9/2}$, $^4F_{9/2}$, $^2H_{11/2}$, $^4F_{7/2}$, $^4F_{5/2}$, $^4G_{9/2}$, and $^4G_{11/2}$ of the excited Er^{3+} ions respectively.⁵²

The glaserite compounds $K_3Y(VO_4)_2$ and $K_3Lu(VO_4)_2$ were also doped with varying concentrations of Nd^{3+} , Yb^{3+} , or Er^{3+} (3, 5, or 8%) to evaluate their potential as hosts for lasing ions. Doping was verified by EDX and absorption spectra shown in Figures 10 and 11. The optical properties according to these

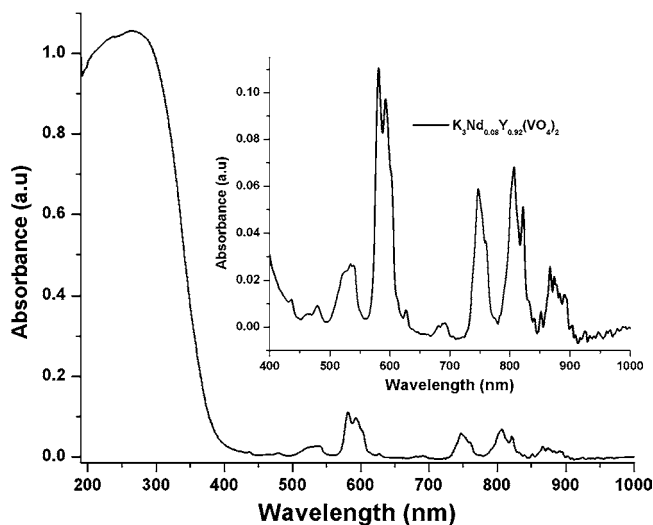


Figure 10. Absorption spectra of $K_3Nd_{0.08}Y_{0.92}(VO_4)_2$ powders in KBr pellets collected at room temperature. The inset shows the expanded area of interest.

dopants (Nd^{3+} , Yb^{3+} , or Er^{3+}) in $K_3Y(VO_4)_2$ were measured by a laser system whose source was non-polarized light. For the $K_3Nd_xY_{1-x}(VO_4)_2$ glaserite material the absorbance ranges obtained were 520–540, 580–600, 745–760, 805–825, and 865–900 nm corresponding to Nd^{3+} ground state absorption to $^2G_{9/2}$, $^4G_{7/2}$, $^2G_{7/2}$, $^4G_{3/2}$ and $^4F_{7/2}$, $^2H_{9/2}$ + $^4F_{5/2}$ energy levels. The highest absorption of $Nd:K_3Y(VO_4)_2$ in KBr pellet was observed in the range of 580–600 nm (Figure 10) and intensity of the absorption peaks increased with increase in the Nd concentration.

Non-polarized absorption spectra of $K_3Er_{0.08}Y_{0.92}(VO_4)_2$ and $K_3Er_{0.08}Lu_{0.92}(VO_4)_2$ are shown in Supporting Information Figures SI 12 and SI 13. The ultraviolet absorption band below 360 nm is attributed to the VO_4^{-3} subunit.^{44,45} The absorption spectrum of $K_3Er_{0.08}Y_{0.92}(VO_4)_2$ consists of nine bands while that of $K_3Er_{0.08}Lu_{0.92}(VO_4)_2$ is slightly less detailed. The absorption peak centered at 971 nm is attributed to the $^4I_{15/2}$ to $^4I_{11/2}$ transition often used to pump the eye safe 1.5 μm emission that subsequently results from the $^4I_{13/2}$ to $^4I_{15/2}$ transition, whose intense absorption appears around 1528 nm (Supporting Information Figures SI 12). The absorption peaks at 377, 452, 488, 521, 551, 656, and 805 nm correspond to transition from $^4I_{15/2}$ to $^4G_{11/2}$, $^4F_{5/2}$, $^4F_{7/2}$, $^2H_{11/2}$, $^4F_{3/2}$, $^4F_{9/2}$ and $^4I_{9/2}$, respectively.⁵²

The non-polarized absorption spectra in Figure 11 is characteristic of a typical near-infrared transition for Yb^{3+} doped inorganic compounds such as $Yb:YVO_4$, $Yb:YAG$, and $Yb:LuVO_4$.^{53,54} The spectra of $K_3Yb_{0.08}Y_{0.92}(VO_4)_2$ and $K_3Yb_{0.08}Lu_{0.92}(VO_4)_2$ show three main absorption features: a small one around 900 nm, a broader transition around 940 nm, and the strong, sharp peak around 970 nm which correspond to $^2F_{7/2}$ to $^2F_{5/2}$ transition in Yb^{3+} ions.⁴⁸ The peak locations due to Yb^{3+} doping in $K_3Yb_{0.08}Y_{0.92}(VO_4)_2$ are found at 903, 945, and 973 nm while those found in $K_3Yb_{0.08}Lu_{0.92}(VO_4)_2$ are 899, 941, and 968 nm respectively. Optical pumping is possible in all these three Yb^{3+} absorption regions. The broad absorption around 940 nm would be most interesting for pumping if coupled with commercially available InGaAs laser diodes, while the sharp absorption peak at 970 nm is more interesting for pump sources with a narrow spectral range like Ti:sapphire lasers. We note that Yb doping in the lutetium host glaserite results in a proportionally larger absorption band at 970 nm compared to 940 nm than is observed in the Yb doped yttrium host glaserite. This could have implications in selection of host materials for future optical applications depending on which pumping arrangement is preferred.

CONCLUSIONS

We report here a new series glaserite compounds with the general formula $K_3RE(VO_4)_2$ ($RE = Sc, Y, Dy, Er, Ho, Tm, Yb$,

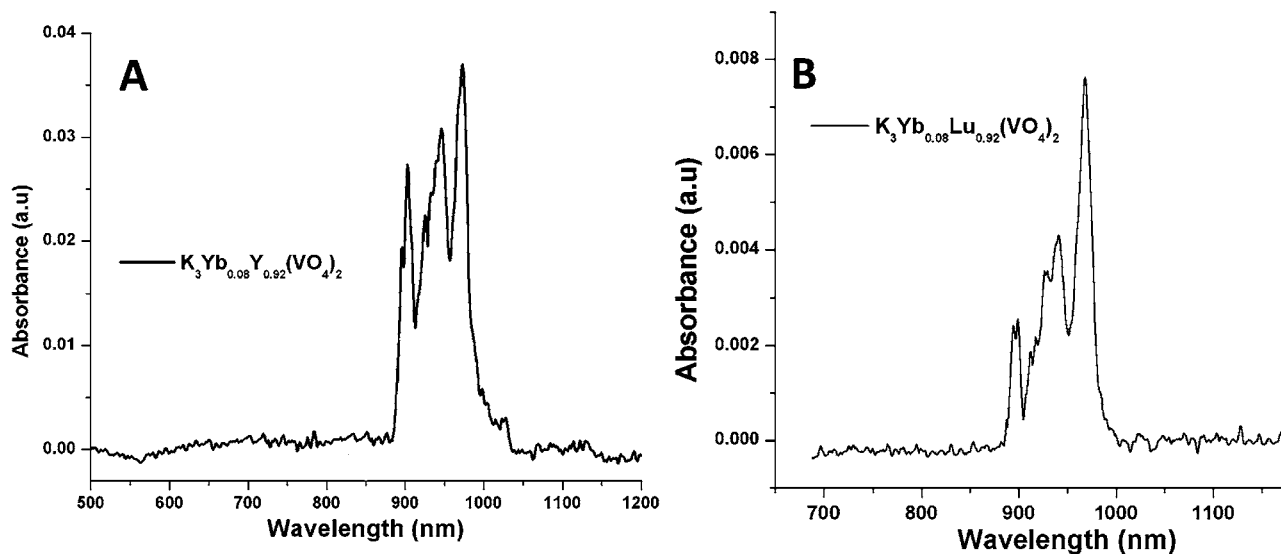


Figure 11. Absorption spectra of (A) $K_3Yb_{0.08}Y_{0.92}(VO_4)_2$ and (B) $K_3Yb_{0.08}Lu_{0.92}(VO_4)_2$ powders in KBr pellets collected at room temperature.

Lu) that have been synthesized hydrothermally and characterized using single crystal X-ray diffraction, powder diffraction, DTA/TGA, Raman, infrared, and absorption spectroscopy. The new glaserite compounds were prepared by a number of methods, but the route that leads to the largest crystals in the greatest quantities uses the solid state reactions of KO_2 , KVO_3 , and RE_2O_3 (RE = Y, Sc, Dy, Er, Ho, Lu, Tm, Yb) in a molar ratio of 1:2:1 in platinum crucibles in air at 1000 °C for 48 h followed by hydrothermal recrystallization in 10 M K_2CO_3 at 560 °C in a sealed silver ampule for 6 days.

These crystals are nonhygroscopic and chemically stable in air and organic solvents such as acetone, and DTA results reveal that $\text{K}_3\text{Y}(\text{VO}_4)_2$ crystals are chemically and thermally stable up to 1250 °C. Attempts to grow other glaserite compounds containing larger lanthanide atoms such as La–Tb were unsuccessful and resulted in the formation of $\text{LnO}(\text{OH})$ and LnVO_4 (where Ln = La–Tb). All the synthesized compounds assume the high symmetry trigonal space group $P\bar{3}m1$, and none were obtained in the previously reported space group $C2/c$ ($\text{K}_3\text{Y}(\text{VO}_4)_2$ (PDF No: 00-049-1227) or $\text{Na}_3\text{Ln}(\text{VO}_4)_2$ (Ln = La, Nd, and Er)) which were grown by high temperature melt flux reactions.

The spectroscopic properties of Er^{3+} , Nd^{3+} , and Yb^{3+} doped potassium double vanadates of the formula $\text{K}_3(\text{Y}/\text{Lu})_{1-x}\text{Ln}_x(\text{VO}_4)_2$ (Ln = Er^{3+} , Nd^{3+} , and Yb^{3+}) were also investigated. The transparent Y and Lu analogues can be used as hosts and dope with a variety of typical lasing ions in a wide range of concentrations. The preliminary results suggest that the materials can act as suitable laser hosts. In particular the absorption spectra of $\text{K}_3\text{Yb}_x\text{Y}_{1-x}(\text{VO}_4)_2$ and $\text{K}_3\text{Yb}_x\text{Lu}_{1-x}(\text{VO}_4)_2$ manifest different splitting, intensities, and peak location of the ${}^2F_{7/2}$ to ${}^2F_{5/2}$ transition in Yb^{3+} . The results presented here show that this new material has considerable potential as a new laser host once good quality crystals are synthesized.

■ ASSOCIATED CONTENT

● Supporting Information

Crystallographic data in CIF format. Further details are given in Figures SI 1–SI 13. This material is available free of charge via the Internet at <http://pubs.acs.org>.

■ AUTHOR INFORMATION

Corresponding Author

*E-mail: kjoseph@clemsun.edu.

Notes

The authors declare no competing financial interest.

■ ACKNOWLEDGMENTS

We are indebted to the National Science Foundation DMR-0907395) for funding and support.

■ REFERENCES

- (1) Vlasse, M.; Parent, C.; Salmon, R.; Le Flem, G.; Hagenmuller, P. *J. Solid State Chem.* **1980**, *35*, 318–324.
- (2) Kaczmarek, M.; Mroz, B. *Phys. Rev. B* **1998**, *57*, 13589–13598.
- (3) Isupov, V. A. *Ferroelectrics* **2005**, *322*, 83–114.
- (4) Kloss, M.; Finke, B.; Schwarz, L.; Haberland, D. *J. Lumin.* **1997**, *72–74*, 684–686.
- (5) Hong, H. Y. P.; Chinn, S. R. *Mater. Res. Bull.* **1976**, *11*, 421–428.
- (6) Kharsika, V. F.; Komissarova, L. N.; Kirichenko, A. N.; Murav'ev, E. N.; Orlovskii, V. P.; Chernyaev, A. P. *Inorg. Mater.* **2001**, *37*, 963–967.

- (7) Legendziewicz, J.; Guzik, M.; Szuszkiewicz, W. *J. Alloys Compd.* **2008**, *451*, 165–171.
- (8) Irena, S. *Thermochim. Acta* **2001**, *370*, 125–128.
- (9) Okada, K.; Ossaka, J. *Acta Crystallogr., Sect. B* **1980**, *36*, 919–921.
- (10) Gossner, B. *Neues Jahrb. Mineral., Abh.* **1928**, *57*, 89–116.
- (11) Tomaszewski, P. E.; Pietraszko, A.; Maczka, M.; Hanuza, J. *Acta Crystallogr., Sect. E* **2002**, *58*, i119–i120.
- (12) Bredig, M. A. *J. Phys. Chem.* **1942**, *46*, 747–764.
- (13) Bredig, M. A. *J. Am. Chem. Soc.* **1941**, *63*, 2533–2533.
- (14) Arumugam, N.; Sofin, M.; Jansen, M. Z. *Kristallogr.-New Cryst. Struct.* **2005**, *220*, 531–532.
- (15) Fabry, J.; Petricek, V.; Vanek, P.; Cisarova, I. *Acta Crystallogr., Sect. B* **1997**, *53*, 596–603.
- (16) Madariaga, G.; Breczewski, T. *Acta Crystallogr., Sect. C* **1990**, *46*, 2019–2021.
- (17) Mogare, K. M.; Klein, W.; Peters, E. M.; Jansen, M. *Solid State Sci.* **2006**, *8*, 500–507.
- (18) Szczygieł, I.; Matraszek, A.; Znamierowska, T. *J. Therm. Anal. Calorim.* **2008**, *93*, 671–676.
- (19) Czupińska, G. *J. Therm. Anal. Calorim.* **2000**, *60*, 199–202.
- (20) Jungowska, W. *J. Therm. Anal. Calorim.* **2000**, *60*, 193–197.
- (21) Salmon, R.; Parent, C.; Le Flem, G.; Vlasse, M. *Acta Crystallogr., Sect. B* **1976**, *32*, 2799–2802.
- (22) Vlasse, M.; Salmon, R.; Parent, C. *Inorg. Chem.* **1976**, *15*, 1440–1444.
- (23) Parent, C.; Fava, J.; Salmon, R.; Vlasse, M.; Leflem, G.; Hagenmuller, P.; Anticfidancev, E.; Lemaitreblaise, M.; Caro, P. *Nouv. J. Chim.* **1979**, *3*, 523–527.
- (24) Macrae, C. F.; Bruno, I. J.; Chisholm, J. A.; Edgington, P. R.; McCabe, P.; Pidcock, E.; Rodriguez-Monge, L.; Taylor, R.; van de Streek, J.; Wood, P. A. *J. Appl. Crystallogr.* **2008**, *41*, 466–470.
- (25) Spek, A. L. *J. Appl. Crystallogr.* **2003**, *36*, 7–13.
- (26) *CrystalClear*; Rigaku & Molecular Structure Corporation: The Woodlands, TX, 2006.
- (27) Sheldrick, G. M. *Acta Crystallogr.* **2008**, *A64*, 112–122.
- (28) Kimani, M. M.; McMillen, C. D.; Kolis, J. W. *Inorg. Chem.* **2012**, *51*, 3588–3596.
- (29) Forbes, A. R.; McMillen, C. D.; Giesber, H. G.; Kolis, J. W. *J. Cryst. Growth* **2008**, *310*, 4472–4476.
- (30) Bobylev, A. P.; Boubentsova, M. N.; Komissarova, L. N.; Ogorodova, L. P.; Spiridonov, F. M. *Mendeleev Commun.* **2004**, *14*, 146–147.
- (31) Abriel, W.; Rau, F.; Range, K. J. *Mater. Res. Bull.* **1980**, *15*, 1099–1104.
- (32) Moore, P. B. *Am. Mineral.* **1973**, *58*, 32–42.
- (33) Hirano, S.; Yogo, T.; Kikuta, K.; Sakamoto, W.; Koganei, H. *J. Am. Ceram. Soc.* **1996**, *79*, 3041–3044.
- (34) Miller, S. A.; Caspers, H. H.; Rast, H. E. *Phys. Rev.* **1968**, *168*, 964–969.
- (35) Yu, M.; Lin, J.; Fang, J. *Chem. Mater.* **2005**, *17*, 1783–1791.
- (36) Frost, R. L.; Palmer, S. J.; Čejka, J.; Sejkora, J.; Plášil, J.; Bahfenne, S.; Keeffe, E. C. *J. Raman Spectrosc.* **2011**, *42*, 1701–1710.
- (37) Frost, R. L.; Henry, D. A.; Weier, M. L.; Martens, W. *J. Raman Spectrosc.* **2006**, *37*, 722–732.
- (38) Bi, C. Z.; Ma, J. Y.; Yan, J.; Fang, X.; Yao, D. Z.; Zhao, B. R.; Qiu, X. G. *Eur. Phys. J. B* **2006**, *51*, 167–171.
- (39) Rousseau, D. L.; Bauman, R. P.; Porto, S. P. S. *J. Raman Spectrosc.* **1981**, *10*, 253–290.
- (40) Frost, R. L.; Palmer, S. J.; Čejka, J.; Sejkora, J.; Plášil, J.; Bahfenne, S.; Keeffe, E. C. *J. Raman Spectrosc.* **2011**, *42*, 1701–1710.
- (41) Griffith, W. P.; Wickins, T. D. *J. Chem. Soc., A* **1966**, 1087–1090.
- (42) Busca, G. *J. Raman Spectrosc.* **2002**, *33*, 348–358.
- (43) Frost, R. L.; Erickson, K. L.; Weier, M. L.; Carmody, O. *Spectrochim. Acta, Part A* **2005**, *61*, 829–834.
- (44) Dzwigaj, S.; Matsuoka, M.; Anpo, M.; Che, M. *J. Phys. Chem. B* **2000**, *104*, 6012–6020.

- (45) Mathieu, M.; Van Der Voort, P.; Weckhuysen, B. M.; Rao, R. R.; Catana, G.; Schoonheydt, R. A.; Vansant, E. F. *J. Phys. Chem. B* **2001**, *105*, 3393–3399.
- (46) Bulánek, R.; Čapek, L.; Setnička, M.; Čičmanec, P. *J. Phys. Chem. C* **2011**, *115*, 12430–12438.
- (47) Čapeka, L.; Adama, J.; Grygarb, T.; Bulánka, R.; Vradmanc, L.; Košová-Kučerová, G.; Čičmaneca, P.; Knoteka, P. *Appl. Catal., A* **2008**, *342*, 99–106.
- (48) Zhang, H.; Yu, Y.; Cheng, Y.; Liu, J.; Li, H.; Ge, W.; Cheng, X.; Xu, X.; Wang, J.; Jiang, M. *J. Cryst. Growth* **2005**, *283*, 438–443.
- (49) Aebersold, M. A.; Guedel, H. U.; Furrer, A.; Blank, H. *Inorg. Chem.* **1994**, *33*, 1133–1138.
- (50) Jamalalah, B. C.; Kumar, J. S.; Suhasini, T.; Jang, K.; Lee, H. S.; Choi, H.; Rama Moorthy, L. *J. Alloys Compd.* **2009**, *474*, 382–387.
- (51) Suresh Kumar, J.; Pavani, K.; Mohan Babu, A.; Kumar Giri, N.; Rai, S. B.; Moorthy, L. R. *J. Lumin.* **2010**, *130*, 1916–1923.
- (52) Gruber, J. B.; Burdick, G. W.; Chandra, S.; Sardar, D. K. *J. Appl. Phys.* **2010**, *108*, 23109–23117.
- (53) Liu, J. H.; Mateos, X.; Zhang, H. J.; Wang, J. Y.; Jiang, M. H.; Griebner, U.; Petrov, V. *Opt. Lett.* **2005**, *30*, 3162–3164.
- (54) He, X. M.; Zhao, G. J.; Xu, X. D.; Zeng, X. H.; Xu, J. *Chin. Opt. Lett.* **2007**, *5*, 295–297.